ACS APPLIED MATERIALS & INTERFACES

Research Article

www.acsami.org

Sealing of Hard CrN and DLC Coatings with Atomic Layer Deposition

Emma Härkönen,*[,†] Ivan Kolev,[‡] Belén Díaz,[§] Jolanta Światowska,[§] Vincent Maurice,[§] Antoine Seyeux,[§] Philippe Marcus,[§] Martin Fenker,[∥] Lajos Toth,[⊥] György Radnoczi,[⊥] Marko Vehkamäki,[†] and Mikko Ritala[†]

[†]Laboratory of Inorganic Chemistry, University of Helsinki, P.O. Box 55, FIN-00014 Helsinki, Finland

[‡]Hauzer Techno Coating BV, 5928 LL Venlo, the Netherlands

[§]Laboratoire de Physico-Chimie des Surfaces, CNRS (UMR 7075), Chimie ParisTech (ENSCP), F-75005 Paris, France

[∥]FEM Research Institute, Precious Metals and Metals Chemistry, D-73525 Schwäbisch Gmünd, Germany

[⊥]Research Centre for Natural Sciences HAS (MTA TKK), 1025 Budapest, Hungary

ABSTRACT: Atomic layer deposition (ALD) is a thin film deposition technique that is based on alternating and saturating surface reactions of two or more gaseous precursors. The excellent conformality of ALD thin films can be exploited for sealing defects in coatings made by other techniques. Here the corrosion protection properties of hard CrN and diamond-like carbon (DLC) coatings on low alloy steel were improved by ALD sealing with 50 nm thick layers consisting of Al_2O_3 and Ta_2O_5 nanolaminates or mixtures. In cross sectional images the ALD layers were found to follow the surface morphology of the CrN coatings uniformly. Furthermore, ALD growth into the pinholes of the CrN coating was verified. In electrochemical measurements the ALD sealing was found to decrease the current density of the CrN coated steel by over 2 orders of magnitude. The neutral salt spray (NSS) durability was also improved: on the best samples the appearance of corrosion spots was delayed from 2 to 168 h. On DLC coatings the adhesion of the ALD sealing layers was weaker, but still clear improvement in NSS durability was achieved indicating sealing of the pinholes.

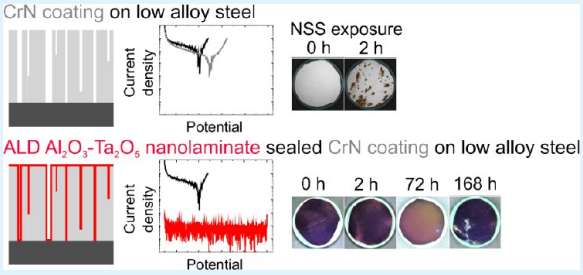

KEYWORDS: *corrosion, coating, sealing, atomic layer deposition, CrN, diamond-like carbon*

1. INTRODUCTION

Physical vapor-deposited (PVD) and plasma-enhanced chemical vapor-deposited (PECVD) hard coatings are widely used for increasing the lifetime of tools and other components under mechanical stress.[1,2] CrN coatings are known for their good mechanical, corrosion and oxidation protection properties,[3−5] and diamond-like carbon (DLC) coatings for their high hardness, low friction and excellent wear resistance.[6−8] Whist the mechanical and intrinsic chemical durability of these coatings is known to be excellent, they suffer from defects.[9−13] Pinholes that extend through the coating and expose the substrate surface to the environment can cause accelerated local corrosion. Several approaches have been proposed to overcome this problem including substrate pretreatment, interlayers and multilayer coatings.[10,14,15]

Atomic layer deposition (ALD) is a chemical vapor deposition (CVD) based method for growing thin films.[16,17] In ALD, the film growth proceeds through alternating and saturating reactions of two or more gaseous precursors on a substrate surface. The growth mechanism ensures that film deposition occurs only on surfaces and thus excellent conformality and uniformity are achieved even on challenging 3D morphologies.[18] Corrosion protection of stainless steel,[19−24] steel,[25−31] aluminum alloy,[25] magnesium alloy,[32] magnesium−lithium alloy,[33] copper,[34,35] and silver[36] with ALD coatings has been studied. Promising results have been obtained with coatings combining the barrier properties of Al_2O_3 with the chemical stability of TiO_2 or Ta_2O_5.[19,23,24,28,30−32,36] However, the growth of ALD thin films is relatively slow, and thus only coatings with submicrometer thicknesses are economically feasible to produce. Because thicker layers are needed against erosive loads, the range of applications for solely ALD based protective coatings is limited.

Combination of hard CrN and DLC coatings with ALD can solve the problems encountered with either coating type alone. While CrN and DLC provide excellent mechanical durability, ALD can be grown on and into defects in these coatings effectively sealing them. A schematic of the sealing of a defective CrN coating with ALD is presented in Figure 1. The basic principle is that a thin ALD layer is deposited into the pinhole defects in the defective thicker coating. Depending on the pinhole dimensions and the ALD layer thickness some pinholes will be completely blocked and some will have

Received: November 4, 2013
Accepted: January 15, 2014
Published: January 15, 2014

   dx.doi.org/10.1021/am404906x | *ACS Appl. Mater. Interfaces* 2014, 6, 1893−1901

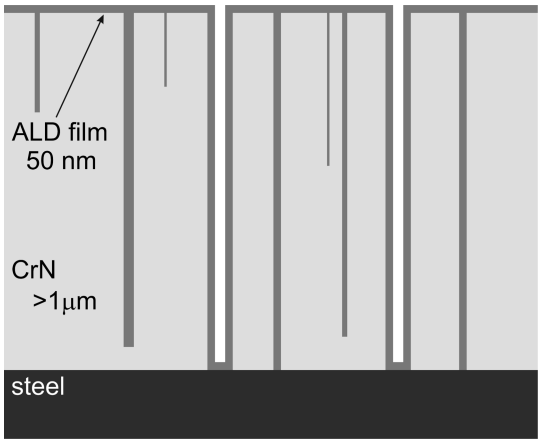

Figure 1. A schematic of the principle of ALD sealing of a CrN coating on steel.

conformal ALD coverage on the pore walls and at the bottom of the pinhole. Shan et al.[37] have shown that the corrosion protection properties of magnetron sputtered CrN coatings on stainless steel can indeed be improved with ALD TiO_2 thin films. Marin et al.[38] have shown improved corrosion protection properties of reactive arc deposited TiN/TiAlN and TiCN coatings on tool steel when sealed with ALD Al_2O_3. Wang et al.[39] have used dual-layer PVD-Al/ALD-Al_2O_3 coatings on Mg-10Li-0.5Zn alloy for corrosion protection. Their aim was to prevent Li-ions from migrating into the ALD Al_2O_3 layer by a PVD-Al interlayer, and thus improve the protective properties of the duplex layer. On the other hand, Härkönen et al.[40] have shown that 10−70 nm filtered cathodic arc deposited (FCAD) interlayers between ALD coatings and steel allow for better control of the coating-steel interface. Thus growth of ALD coatings with better barrier properties and significantly enhanced durability was enabled.

In this study, the corrosion durability of a low alloy steel coated with unbalanced magnetron (UBM) sputtered CrN and PECVD DLC coatings were improved by ALD Al_2O_3−Ta_2O_5 nanolaminate, $Al_xTa_yO_z$ mixture and graded mixture sealing layers. The ALD layers were chosen based on earlier work.[28,30,31,40] ALD Al_2O_3 is an excellent insulator and nucleates well on various kinds of surfaces,[26,28] but does not provide sufficient durability against a chemical attack.[27] ALD Ta_2O_5, on the other hand, is chemically stable, but does not nucleate as well as Al_2O_3.[28,29] Carefully optimized combination of the two materials into nanolaminates or mixtures has been shown to provide good barrier properties with sufficient durability against chemical attack.[28,30] The influence of the ALD sealing to corrosion protection properties was studied with electrochemical methods and neutral salt spray (NSS) testing. Additionally, the morphology and in-depth composition of the combined coatings were examined to gain insight into the mechanism behind the improved corrosion durability.

2. EXPERIMENTAL METHODS

The corrosion protection coatings were grown on low alloy steel (AISI 52100, DIN 100Cr6). The composition of the steel (in wt.%) was C (0.95−1.1), Cr (1.5), Ni (max. 0.30), Mn (0.25−0.45), Cu (max. 0.30), Si (0.15−0.35), P (max. 0.030), S (max. 0.025), and Fe (balance). The steel samples were hardened and tempered at 180 °C resulting in a final hardness of 805 HV. Prior to coating most of the substrates were lapped in a water based diamond suspension (6 μm) and brushed. Steel samples coated with unsealed CrN and DLC and used for neutral salt spray (NSS) testing, were fine ground.

CrN and DLC coatings were deposited on the low alloy steel with Hauzer Techno Coating BV equipment (Hauzer Flexicoat 1200). The CrN coating was deposited by UBM DC sputtering at 180 °C temperature. The DLC coating consisted of three subsequent layers: Cr, W−C:H, and DLC (a−C:H). The inner Cr and W−C:H layers were deposited by UBM sputtering and the topmost DLC layer by PECVD at temperatures lower than 200 °C. Prior to coating the samples were cleaned in an industrial cleaning line. Both CrN and DLC were grown in two thicknesses as indicated in Table 1.

Table 1. Coding and Nominal Thicknesses of Studied Coatings on Steel

code	hard layer	ALD sealant
CrN2	2.44 μm CrN	
DLC3	2.85 μm Cr+W−C:H +DLC	
CrN2-laminate	2.44 μm CrN	2 × [12.5 + 12.5] nm Al_2O_3−Ta_2O_5 nanolaminate
CrN1-mixture	1.05 μm CrN	50 nm $Al_xTa_yO_z$ mixture
CrN2-mixture	2.44 μm CrN	50 nm $Al_xTa_yO_z$ mixture
CrN1-graded	1.05 μm CrN	50 nm $Al_xTa_yO_z$ graded mixture
CrN2-graded	2.44 μm CrN	50 nm $Al_xTa_yO_z$ graded mixture
DLC3-laminate	2.85 μm Cr+W−C:H +DLC	2 × [12.5 + 12.5] nm Al_2O_3−Ta_2O_5 nanolaminate
DLC2-mixture	2.35 μm Cr+W−C:H +DLC	50 nm $Al_xTa_yO_z$ mixture
DLC3-mixture	2.85 μm Cr+W−C:H +DLC	50 nm $Al_xTa_yO_z$ mixture
DLC2-graded	2.35 μm Cr+W−C:H +DLC	50 nm $Al_xTa_yO_z$ graded mixture
DLC3-graded	2.85 μm Cr+W−C:H +DLC	50 nm $Al_xTa_yO_z$ graded mixture

After coating the samples with CrN and DLC, the samples were exposed to ambient environment. To ensure the least possible contamination at the interface between the ALD and CrN or DLC layers, cleaning was done again prior to the ALD process: The samples were wiped with a precision wipe drenched in acetone, ultrasonicated for 5 min in acetone and isopropanol, rinsed with ethanol and blow-dried with compressed air. Finally, the samples were H_2−Ar plasma treated in a Beneq TFS-200 ALD reactor for 30 min to decrease hydrocarbon contamination. The detailed procedure is presented in a previous publication.[31] The temperature was 160 °C, and the treatment was executed by ALD-type pulsing (5 s on and 10 s off). The cycle was repeated 360 times to reach the desired 30 min treatment time. A capacitively coupled 13.56 MHz rf power source was used for generating the plasma, and the reactor was operated in a remote plasma configuration. The plasma power was 170 W. The plasma gas flows for H_2 (>99.999%) and Ar (>99.999%) were maintained at 15 and 130 sccm. The treatment was conducted ex situ: after the treatment the reactor was cooled down to 100 °C, opened to normal laboratory air and the samples were moved to another reactor for the ALD sealing layer deposition. During the transfer the samples were exposed for approximately 2−3 min to laboratory air.

A Picosun SUNALE R-150 ALD reactor was used for growing the sealing layers. The process parameters are detailed in previous publications.[28,30,40] The depositions were done at 160 °C in approximately 5 mbar pressure. The Al_2O_3 and Ta_2O_5 precursors were trimethyl aluminum (TMA, $Al(CH_3)_3$, Chemtura AXION PA 1300), tantalum pentaethoxide ($Ta(OC_2H_5)_5$, SAFC Hitech) and ultrapure water (H_2O, resistivity >18 MΩ cm). The $Ta(OC_2H_5)_5$ source temperature was 140 °C, and TMA and H_2O were evaporated at room temperature. One cycle in Al_2O_3 deposition sequence

consisted of 0.1 s TMA pulse, 5 s purge, 0.1 s H_2O pulse and 5 s purge. Similarly, the Ta_2O_5 deposition sequence was 0.4 s $Ta(OC_2H_5)_5$ pulse, 5 s purge, 0.4 s H_2O pulse, and 5 s purge. The growth rates of Al_2O_3 and Ta_2O_5 were 0.09 nm/cycle and 0.04 nm/cycle, respectively. Appropriate number of cycles was used to reach the targeted thickness of 50 nm.[28,30,40] The Al_2O_3−Ta_2O_5 nanolaminate was made by repeating the sequence of 12.5 nm Al_2O_3 and 12.5 nm Ta_2O_5 twice. For the $Al_xTa_yO_z$ mixture a sequence of one ALD cycle of Al_2O_3 and three cycles of Ta_2O_5 was repeated. The graded $Al_xTa_yO_z$ mixture was deposited by starting with a bare Al_2O_3 layer, followed by a compositionally changing mixture layer and finally ending with a bare Ta_2O_5 layer. In the middle section the cycling sequence was continuously changed to produce an increasing Ta_2O_5 concentration toward the surface. For process control, a piece of silicon wafer was included in each ALD run.

The coatings, their coding and nominal thicknesses are presented in Table 1. The hard coatings are named by the acronyms of the coating materials and the ALD sealing layers by the type of the coating architecture.

The surface morphology of the coatings without and with ALD sealing was studied with field emission scanning electron microscopy (FESEM, Hitachi S-4800). Cross sectional imaging was done with transmission electron microscopy (TEM, Philips CM20). The cross sectional samples were fabricated by cutting the samples, embedding into a Ti-holder, mechanically grounding and polishing, and finally milling with 10 keV Ar^+-ions. To minimize the damage to the samples, the final milling step was done at a lower voltage of 3 keV.

The efficiency of the ALD sealing of pinholes in the CrN coating was evaluated from cross-sectional images. A defect site was chosen from the surface of the CrN coating and focused ion beam (FIB) milling was used to create a cross section of the area. Thereafter energy dispersive X-ray spectrometry (EDS) was used for recording elemental maps on the cross section. A FEI Quanta 3D 200i Dual-Beam FIB/SEM microscope equipped with an Omniprobe nanomanipulator was used for lift-out preparation. An Oxford Instruments X-max 50 mm^2 SSD Detector with INCA 350 Analyzer was used for the EDS mapping. The EDS measurement was done with a 5 kV electron beam in order to improve the EDS surface sensitivity and spatial resolution. The maps on the cross section were analyzed for Pt (M_α line), Ga (L_α line), Al (K_α line), Ta (M_α line), O (K_α line), Cr (L_α line), N (K_α line), and Fe (L_α line).

The composition of a CrN coating sealed with ALD mixture was depth profiled with time-of-flight secondary ion mass spectrometry (ToF-SIMS, Iontof ToF-SIMS 5 spectrometer). The measurement was done with a pulsed 25 keV Bi^+ primary ion source delivering 1.3 pA of analysis current over a 100 × 100 μm^2 area. The depth profiling was done by sputtering with a 1 keV Cs^+ beam giving a target current of 60 nA over a 300 × 300 μm^2 area. Negative ion profiles were used. The operation pressure was 10^{-9} mbar. Ion-Spec software was used for the data acquisition and postprocessing.

The electrochemical properties of 2.44 μm CrN coatings without and with ALD sealing were evaluated with polarization (linear sweep voltammetry) measurements. An AUTOLAB PGSTAT30 potentiostat/galvanostat was used for the measurements. The electrolyte solution was 0.2 M NaCl (Analar Normpur analytical reagent VWR BDH Prolabo) at pH 7 and room temperature. The electrolyte was bubbled with Ar 30 min prior to the measurement and the bubbling was continued throughout the measurement. A traditional three-electrode setup was used with platinum counter electrode and standard calomel electrode (SCE) reference. All given potentials are versus the SCE. The measurement was started with a 30 min open circuit potential (OCP) measurement to ensure system stability, and the measurement range was from −0.9 to 0.0 V or until the current density exceeded 10 $\mu A\ cm^{-2}$. The scan rate was 1 $mV\ s^{-1}$. The exposed sample area was limited to 0.44 cm^2 with a Viton O-ring. No polarization measurements were conducted on DLC coatings without or with ALD sealing, because the adhesion between the DLC and ALD layers appeared to be insufficient. Visible peeling off of the ALD layers was observed, as discussed in detail in sections covering the results on the DLC coated samples (section 3.2.).

Corrosion durability evaluation was done with NSS testing. The procedure was executed according to standard DIN 50021 (ISO 9227) except that the samples were photographed at regular intervals. Prior to photography the samples were rinsed with deionized water. During NSS the temperature, pH and NaCl concentration were constant at 35 ± 2 °C, 6.5−7.2 and 50 ± 5 g/L, respectively. Rust grading was given to the samples after 2, 4, 24, 48, 72, 168, and 336 h of testing according to standard DIN 51802 (Table 2). Percentages for rust grade evaluation were determined according to Renault standard D17 1058J. The sample surfaces were divided into 4 × 4 mm squares. Squares that were over 50% filled by the sample were considered in the analysis. Each square was evaluated separately and the percentage of corroded area was obtained by considering the number of corroded squares against the total number of squares. A square was considered corroded if even one corrosion spot could be found in it. The testing was conducted with 1−4 samples per coating type covering coatings with all deposited thicknesses.

Table 2. Definition of Rust Grades According to Standard DIN 51802

rust grade	description of the rust figure	area of corrosion (%)
0	no corrosion	0
1	max. three corrosion spots covering less than 1 mm^2	not defined
2	slight corrosion	<1
3	moderate corrosion	1−5
4	heavy corrosion	5−10
5	very heavy corrosion	>10

3. RESULTS AND DISCUSSION

3.1. Sealing of CrN Coatings. *3.1.1. Morphology and Composition.* FESEM images of steel coated with CrN and ALD mixture sealed CrN are presented in Figure 2. With the

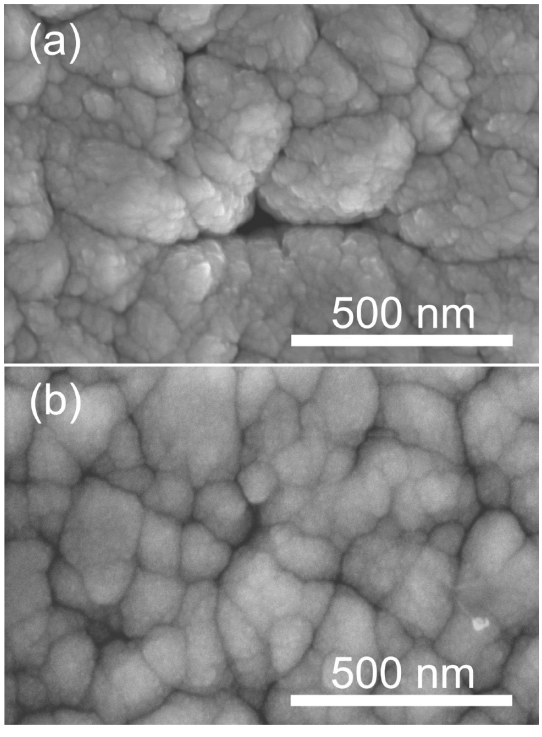

Figure 2. FESEM images of steel coated with CrN (CrN2) (a) and CrN with ALD mixture sealing (CrN2-mixture) (b).

unsealed CrN coating the surface appears rough and the coating seems to consist of columns tightly packed together (Figure 2a). However, in between some columns pinhole defects can be observed. Particles can also be seen on and embedded into the CrN coating (not shown). PVD CrN coatings are known to contain through-coating defects that can connect the substrate to the surrounding environment.[9,11] All features observed on the CrN coated samples are also seen on the ALD sealed samples (Figure 2b). The ALD layer only smoothens the surface appearance and makes the holes smaller due to conformal coverage. Although pinholes can be seen also on the surface of the ALD sealed sample, it is expected that the ALD layer covers the pore walls and the steel surface possibly exposed at the bottom of the holes (c.f., Figure 1). The pinholes that can be seen still after the ALD sealing were originally too large for complete filling with the 50 nm thick ALD layer.

The conformal coverage of CrN by the ALD mixture was confirmed with TEM (Figure 3). The ALD sealing layer follows

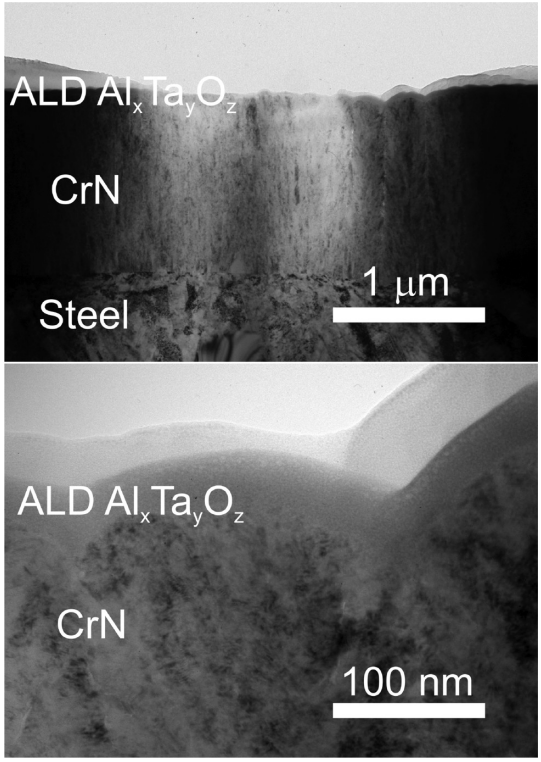

Figure 3. TEM cross-sectional bright-field images of steel coated with ALD mixture sealed CrN (CrN1-mixture) with two magnifications.

the roughness of the CrN coating closely, the layer thickness is constant and no defects can be observed in the local analysis. Additionally the CrN coating appears well adhered to the steel substrate and the ALD layer to the CrN coating.

The conformality of the ALD layer was studied further by making a cross section of a defective site in the CrN coating. From a top-view image a particle was chosen and cross-sectioned with a Ga-ion beam. Thereafter a cross-sectional SEM image and EDS maps were recorded of the defective site (Figure 4). On top of the cross-section clear signals of Pt, used as a mask layer, and Ga, used both for mask layer deposition and FIB milling of the sample, can be observed. The steel surface can be seen at the bottom of the cross section in the Fe

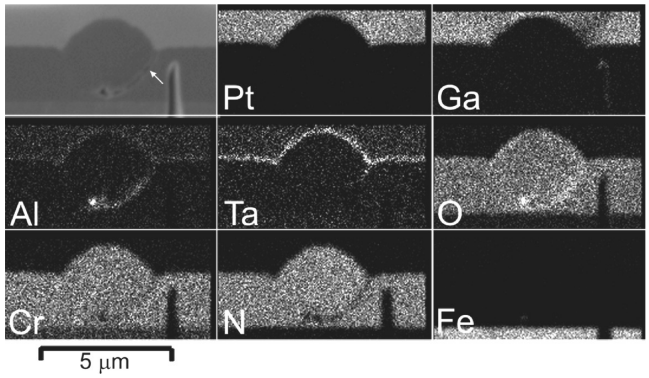

Figure 4. SEM image and EDS maps on a cross section of a defective site in the ALD mixture sealed CrN coating (CrN2-mixture). The arrow in the SEM image points the defective site in the CrN coating.

map. The CrN coating sealed with the ALD mixture lies in the middle. The Al and Ta maps show a clear layer at the top of the CrN coating. Additionally, Al and Ta can be seen to penetrate into the CrN coating along the side of the particle. In the area of Al and Ta penetration a corresponding low intensity can be seen in the Cr and N maps. This shows that the ALD layer sealed efficiently the CrN coating and penetrated into the pinhole defects. The O map seems to show a relatively high concentration of oxygen throughout the CrN coating, but this is due to the overlapping O and Cr peaks, and thus does not indicate significant oxidation of the CrN coating. Based on the Al and Ta maps, Al_2O_3 appeared to penetrate further down into the pinhole than Ta_2O_5. The defects are high aspect ratio features and upon filling their aspect ratios increase toward infinity. Coating such high aspect ratio structures even with ALD is challenging and requires high precursor doses. Gordon et al.[41] have shown that the precursor exposure needed for conformal coverage scales with the aspect ratio to the power of two. The exposure is given by a product of partial pressure of the precursor and exposure time i.e. pulse time. The vapor pressure of TMA at 293 K (the evaporation was done at approximately 298 K) is 1215.8 Pa[42] and the vapor pressure of $Ta(OC_2H_5)_5$ at 418 K (the evaporation was done at 413 K) is 13 Pa,[43] thereby explaining the difference in Al_2O_3 and Ta_2O_5 penetration depths.

ToF-SIMS depth profile of the ALD mixture sealed CrN coating on steel is presented in Figure 5. The ALD sealing layer appears similar in composition as the corresponding ALD mixture in the duplex FCAD/ALD coatings on steel.[40] The dominant signals are the TaO_2^- and AlO_2^- that are

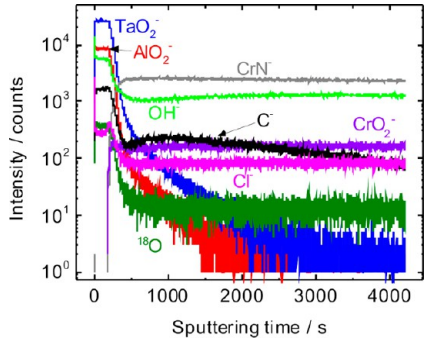

Figure 5. ToF-SIMS depth profile of CrN coating sealed with ALD mixture (CrN2-mixture).

dx.doi.org/10.1021/am404906x | ACS Appl. Mater. Interfaces 2014, 6, 1893−1901

characteristic of the oxide matrix, but also carbon (C^- ions), hydroxyl (OH^- ions) and chlorine (Cl^- ions) impurities are measured in agreement with the previous work.[28,30,40] Negative ion ToF-SIMS is very sensitive to chlorine: in the previous works the chlorine contamination found with it in ALD Al_2O_3 and Ta_2O_5 coatings was below the detection limit of X-ray photoelectron spectroscopy (XPS, 0.5 at.%).[27,29] The CrN layer is taken to start with the increase of the characteristic CrN^- signal. The layer contains also carbon (C^- ions), oxygen ($^{18}O^-$ ions) and chlorine (Cl^- ions) trace impurities. The origin of the Cl^- impurity in the CrN layer is hitherto unknown, but because of the sensitivity of ToF-SIMS, it must be minute. Slight oxidation of the CrN is indicated by the chromium oxide (CrO_2^- ions) signal that is constant through the depth profile. The interface between the ALD and CrN layers appears to be quite free of contamination, as no peaking is observed in the C^- and OH^- signals. Only a slight increase of Cl^- can be seen. Furthermore, a striking feature is that the ALD TaO_2^- and AlO_2^- signals extend into the CrN layer indicating that defect sites in CrN are filled with ALD. This confirms penetration of the ALD layer into the defects in the CrN coating as already observed with EDS in the cross sectional sample (Figure 3). Signals of Fe^- or FeO_2^- cannot be seen in the depth profile implying that the steel substrate was not reached.

3.1.2. Electrochemical Properties. The electrochemical properties of 2.44 μm thick CrN coatings without and with ALD sealing were evaluated with polarization measurements in 0.2 M NaCl solutions at pH 7. The measured polarization curves are presented in Figure 6. On uncoated steel the anodic reaction appears to be under activation control.[44] This is expected due to the low Cr content of the steel alloy (1.5 wt. %), which does not allow passive layer formation on the steel surface. The cathodic reaction is oxygen reduction near the corrosion potential and hydrogen reduction at low potentials.[44] The oxygen reduction is under diffusion control due to the low oxygen concentration in the Ar bubbled electrolyte solution. The hydrogen reduction reaction is activation controlled. The polarization curve for the CrN coated steel shows a slight increase of the corrosion potential, but not large enough to imply simple CrN response to polarization (Figure 6).[45] This indicates that mixed behavior of the CrN coating and steel exposed at the bottom of pinholes in the coating is seen. However, in the studied potential range the CrN coating is chemically inert.[46−48] Thus the corrosion rate of the coating can be considered negligible compared to the corrosion rate of the steel exposed through defects, which is further accelerated by the galvanic coupling of the CrN coating and steel.[46−48]

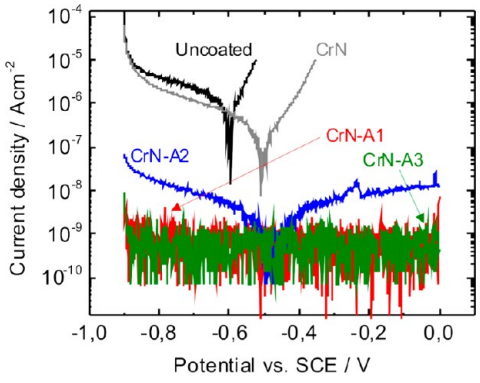

Figure 6. Polarization results of uncoated steel, steel coated with CrN (CrN2) and CrN with ALD nanolaminate (CrN2-laminate), mixture (CrN2-mixture), and graded mixture (CrN2-graded) sealing.

Distinctly different polarization curves were obtained for the steel samples coated with the ALD sealed CrN coatings (Figure 6). The current density is over 2 orders of magnitude lower. This decrease is consistent with conformal sealing of the entire samples, including the lateral top surfaces and the pinholes, with the insulating ALD layers. The sample with the ALD mixture sealed CrN has a similar corrosion potential as the sample with the unsealed CrN coating (Figure 6). The passive-like behavior observed in the anodic potential range for this sample is assigned to the accumulation of substrate corrosion products at the bottom of some pinholes not perfectly closed by the ALD sealant.[29,30] The ALD nanolaminate and graded mixture layers show even better sealing properties (Figure 6). The samples have very low current densities and thus a significant amount of noise in the whole potential range measured. The current density appears to be close or below the detection limit of the equipment used for the measurements. Therefore determination of the corrosion potential or current density was not possible. However, the very low current densities indicate excellent sealing of the whole CrN-steel system including the defects in the CrN coating.

Marin et al.[38] obtained similar results with 4 nm ALD Al_2O_3 sealing of PVD TiAlN/TiN and TiCN coatings. The ALD layer decreased the corrosion current density of the TiAlN/TiN coated sample by almost 1 order of magnitude and the TiCN coated sample by almost 2 orders of magnitude. Also a passive region was provided. Wang et al.[39] showed that on Al-coated Mg−10Li−0.5Zn alloy a 40 nm ALD Al_2O_3 decreased the corrosion current density of the Al-coated alloy by 1 order of magnitude and increased the corrosion potential by 340 mV. Although these results obtained with the ALD Al_2O_3 sealing were very promising, the stability of the sealing layers was not considered. ALD Al_2O_3 is known to be unstable in aggressive solutions, especially on electrochemically active substrates.[27,49] On the other hand, Shan et al.[37] succeeded in increasing the corrosion potential of a CrN coated stainless steel by 250 mV and in decreasing the corrosion current density by almost 1 order of magnitude with 90 nm ALD TiO_2 sealing. TiO_2 is known to be chemically inert and thus would seem to be a better choice for long-term corrosion protection. However, it has poorer barrier properties than Al_2O_3,[19] which makes the sealing less efficient. Better electrochemical barrier properties were achieved in the present work with all the ALD sealing layers combining the barrier properties of Al_2O_3 with the chemical stability of Ta_2O_5. In particular the corrosion current density was lowered by at least 2 orders of magnitude indicating significantly lower corrosion rates. Furthermore, on the basis of previous work[27,28,30,40] also a better long-term durability in aggressive environments is expected with the layers combining Al_2O_3 and Ta_2O_5.

3.1.3. Corrosion Durability. The corrosion durability and long-term stability of the CrN and ALD sealed CrN coatings on steel were studied with NSS testing. The results were analyzed by visual observation (Figure 7) and quantitative rust grades from zero to five (Table 3). A rust grade of zero indicated a surface that had no corrosion spots and a rust grade of 5 a surface that had corrosion on more than 10% of the surface area according to the methodology described in the Experimental Methods section. The number of samples included in the analysis is indicated in Table 3.

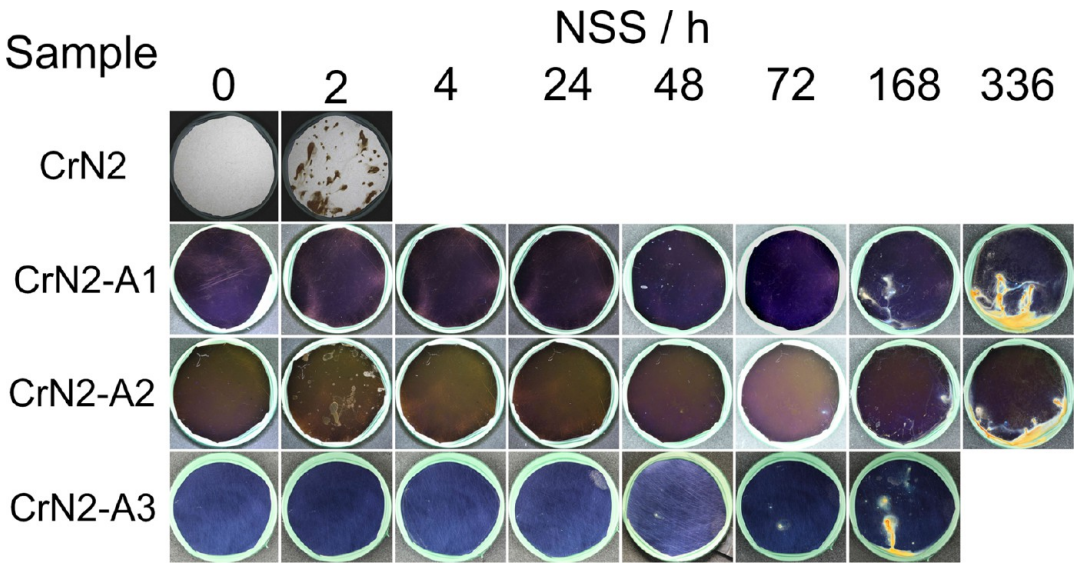

Figure 7. Representative NSS test results of steel coated with 2.44 μm CrN (CrN2) and 2.44 μm CrN sealed with ALD nanolaminate (CrN2-laminate), ALD mixture (CrN2-mixture), and ALD graded mixture (CrN2-graded) layers.

Table 3. Rust Grades of Steel Protected with 1.05 and 2.44 μm Thick CrN without and with ALD Sealing during NSS Testing[a]

	NSS rust grades						
code	2 h	4 h	24 h	48 h	72 h	168 h	336 h
CrN2	5/5						
CrN2-laminate	0/0	0/0	0/0	0/0	0/0	0/5	5/5
CrN1-mixture	0/0	0/0	0/1	0/4	0/5	4/5	5/5
CrN2-mixture	0/0	0/0	0/0	1/0	1/0	5/1	5/5
CrN1-graded	0/0	0/0	0/1	1/1	1/4	4/5	5/5
CrN2-graded	1	5					

[a]The grades determined for each sample are separated by a slash sign.

The steel samples coated with unsealed CrN coating corroded heavily in 2 h of NSS exposure and had a rust grade of 5 (Figure 7 and Table 3). All the ALD sealing layers drastically improved the durability of the CrN coated samples. The best samples remained corrosion free until 168 h and after 336 h large areas on the samples were still intact. Even the worst sample (CrN2-graded) showed only some corrosion after 4 h. Except for this one sample, excellent sealing was achieved with all the ALD layers on CrN as was indicated already by the polarization results. Some variation was observed in the durabilities of samples with in principle identical coatings. This implies that although ALD sealing can be very effective, the consistency should be further improved. Because the coatings survived over large areas, it appears that the variation was mainly caused by impurities and foreign particles incompletely removed by the pre- or midtreatments. No clear indication whether the thickness of the CrN influenced the NSS durability could be drawn. Good behavior was observed with both 1.05 and 2.44 μm thick ALD sealed CrN coatings. Similar behavior was observed also with all the ALD sealing layers (Figure 7 and Table 3). The Al_2O_3–Ta_2O_5 nanolaminate appeared to give slightly better results than the mixture layers. The ALD layers combining Al_2O_3 with Ta_2O_5 have been previously determined to have both excellent barrier properties and durability in aggressive chloride containing environments.[28,30,40] Therefore, it was not surprising that all the studied ALD sealing layers performed well in sealing the CrN coatings.

3.2. Sealing of DLC Coatings. *3.2.1. Morphology and Composition.* The DLC coated steel samples without and with the ALD sealing appeared to contain fewer morphological heterogeneities compared to the CrN counterparts (Figure 8). The surface was smoother, appeared to contain no holes and considerably fewer particles were visible. It should be remembered, however, that also DLC coatings are known to contain through-coating porosity.[12,13] The size of the pores has been evaluated to be in the order of nm,[12,13] and thus may be

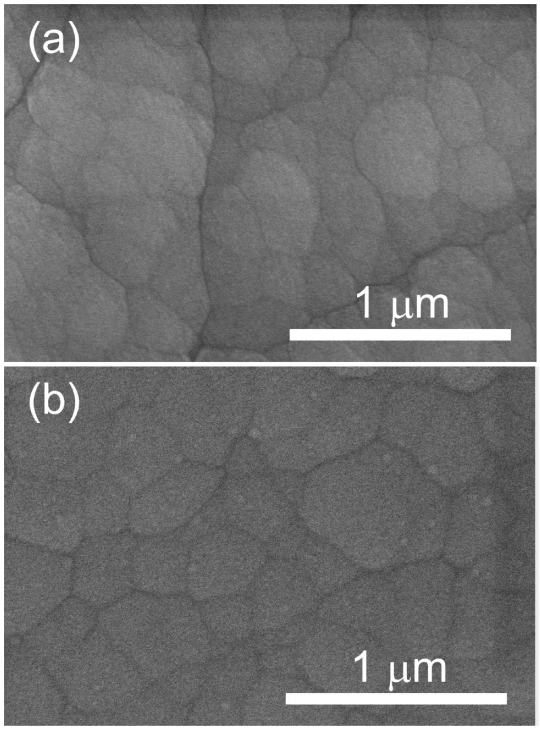

Figure 8. FESEM images of steel coated with DLC (DLC2) (a) and DLC with ALD mixture sealing (DLC2-mixture) (b).

beyond the resolution of FESEM evaluation. Some coated scratches, possibly from the mechanical surface pretreatments, could be seen. As on CrN, the ALD sealing layers appeared to conformally cover the DLC coating, and no defects could be seen.

In TEM cross-sectional images surprisingly no ALD layer could be found on the DLC coated samples (Figure 9). In all the studied coatings the ALD layer appeared to have peeled off. This was also seen in the NSS tested samples (Figure 10).

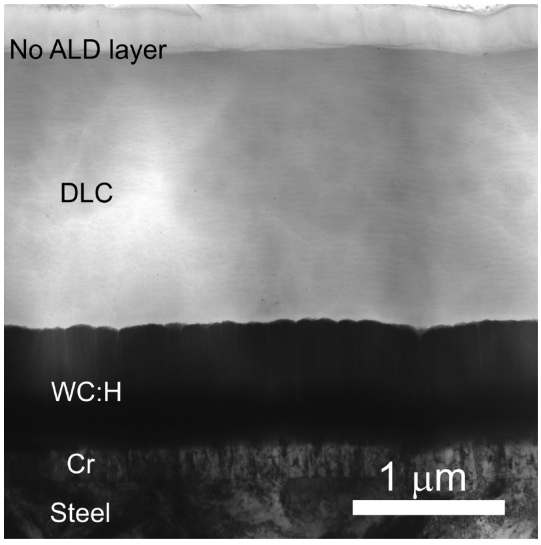

Figure 9. TEM cross-sectional bright-field image of steel coated with ALD mixture sealed DLC (DLC3-mixture).

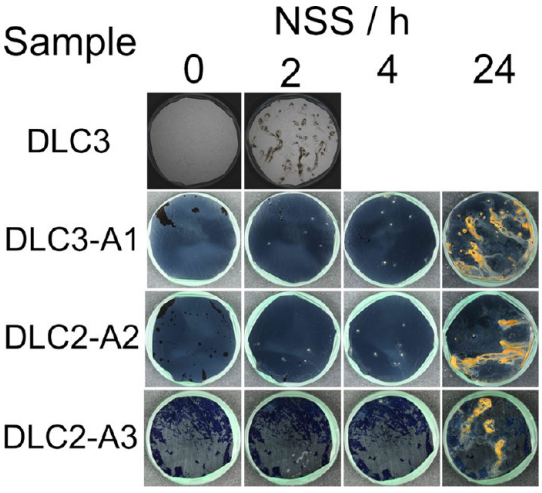

Figure 10. Representative NSS test results of steel coated with 2.85 μm DLC (DLC3), 2.85 μm DLC sealed with ALD nanolaminate (DLC3-laminate), and 2.35 μm DLC sealed with ALD mixture (DLC2-mixture) and ALD graded mixture (DLC2-graded) layers.

Large pieces of the ALD layer had visibly detached while some areas still had the ALD layer. The FESEM analysis was done directly after growing the ALD layers, whereas TEM and NSS were conducted in other laboratories, to which the samples were delivered packed between two polyurethane membranes in a plastic box. The samples stuck slightly to the membranes, and thus the adhesion of the coatings became "tested" when removing the samples from the box. The adhesion problems were probably because of a weak bonding of the ALD layers to the DLC coating. ALD growth starts with reactions between the precursors and the surface to be coated.[16,17] Carbon and hydrocarbon surfaces have been found particularly challenging for ALD. Organic layers have been widely used for surface passivation for selective area ALD[50,51] and carbonaceous impurities on steel surfaces have been shown to significantly decrease the protective properties of ALD coatings.[31] Additionally, ALD growth on carbon nanotubes and graphene has succeeded only after the surfaces have been properly activated.[52−54] DLC films consists mainly of sp^3 and sp^2 hybridized carbon with a deposition method dependent amount of hydrogen.[55,56] Even though the surface of the amorphous DLC contains several surface sites that enable the ALD growth, proper nucleation and chemical bonding to the substrate was probably inhibited leading to the observed weak adhesion of the layers.

3.2.2. Corrosion Durability. The corrosion durability of the DLC coated steel without and with the ALD sealing was tested with NSS similarly to the CrN coatings. The DLC coated steel samples corroded heavily already after 2 h of testing and had a rust grade of 5.0 (Figure 10 and Table 4). No clear difference between the stability of CrN or DLC coated steel could be observed even though the DLC coating appeared smoother and more homogeneous in FESEM (Figures 2 and 8). This confirms that defects connecting the surrounding environment with the steel surface existed also on the DLC coated sample.

The samples coated with DLC and sealed with ALD showed mixed behavior in NSS exposure (Figure 10 and Table 4). On most of the samples the ALD layer was visibly peeled off on some areas due to the weak adhesion discussed above (section 3.2.1.). However, in spite of this the NSS durability of the DLC coated samples was clearly improved with the ALD sealing. Out of 11 samples tested in total, only three had a rust grade of 5 after two hours of testing, and on most samples only corrosion spots instead of bleeding was observed after 24 h of testing. However, as was seen with the ALD sealed CrN coatings, also with the DLC coatings the durabilities of in principle identical samples varied. Due to the problems with adhesion, this variation was more pronounced on the DLC coatings. Nevertheless, on some samples sealing was observed also in areas where the ALD layer had peeled off from the top surface. This can be seen clearly in Figure 10 where corrosion on areas where the ALD layer had peeled off did not occur any sooner than on the other areas of the sample. Remarkably, one ALD graded mixture sealed DLC coating showed excellent behavior (Figure 11). The sample was completely corrosion free even after 504 h of testing and had only a few separate corrosion spots after 672 h. This indicates that even though the adhesion of the ALD layers on top of the DLC coating was inadequate, significant sealing of pinholes was still achieved. These results lead to a suggestion that mechanical locking of the ALD layers in the pinholes improves their adhesion there and thereby enables efficient sealing despite the adhesion failures on the top surface. No clear indication of achieving improved behavior with the thicker 2.85 μm DLC was observed. Thus the NSS durability is suggested to be dependent on the efficiency of the ALD sealing.

4. CONCLUSIONS

Defects in hard CrN and DLC coatings on low alloy steel were successfully sealed with 50 nm thick ALD Al_2O_3−Ta_2O_5 nanolaminate, $Al_xTa_yO_z$ mixture and $Al_xTa_yO_z$ graded mixture

Table 4. Rust Grades of Steel Protected with 2.35 or 2.85 μm DLC without and with the ALD Sealing during NSS Testing[a]

	NSS rust grades						
code	2 h	4 h	24 h	48 h	72 h	168 h	336 h
DLC3	5/5						
DLC3-laminate	5/5						
DLC2-mixture	0/0/0/1	1/0/5/4	5/0/5/5	5/0/5/5	NA	5/5/5/5	
DLC3-mixture	1/5	5/5					
DLC2-graded	0/0	0/4	5/5				
DLC3-graded	0	0	0	0	0	0	0

[a]The grades determined for each sample are separated by a slash sign.

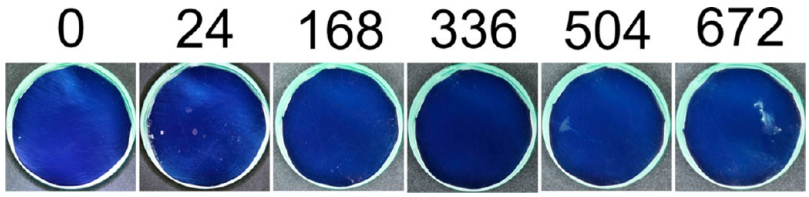

Figure 11. Images of steel coated with ALD graded mixture sealed 2.85 μm DLC (DLC3-graded) after different times (hours) of NSS exposure.

layers. On CrN the ALD layers were observed to smoothen the overall appearance and decrease the size and number of pinhole defects on the surface. The conformal coverage of the CrN coating with ALD was proven with TEM, and the penetration of the ALD layers into the defects was shown with EDS analysis on a cross-section of a pinhole site at a defective growth particle and ToF-SIMS depth profiling. In polarization measurements the current density was decreased by over 2 orders of magnitude in the whole potential range further demonstrating the sealing capabilities of ALD. The NSS durability of the CrN coated steel was also significantly increased: the appearance of first corrosion spots was delayed from 2 to 168 h with the best samples. Compared to previous works on ALD sealing of PVD coatings,[37−39] here the further enhanced barrier properties and long-term durability were attributed to the combination of Al_2O_3 and Ta_2O_5 in the sealing layers.

The sealing of DLC coatings with ALD layers was found to be more challenging. In NSS the ALD sealed samples showed improved durability, but repeatability was an issue. Mixed results were obtained because of the weak adhesion between the ALD layer and the DLC coating. This was attributed to unideal ALD nucleation on the DLC surface leading to insufficient chemical bonding between the layers. Despite this clear sealing of pinholes was observed. It appeared that the ALD layer stuck to the pinhole walls, possibly due to mechanical locking, even when the surface layer was partially detached. Thus significant improvement of both the CrN and DLC corrosion protection properties were obtained with the ALD sealing layers. Careful attention should, however, be given to the starting surface for the ALD growth. Reliable performance can be obtained only on a clean surface and only when appropriate chemical entities that enable good ALD nucleation exist or the surface is activated to have them.

AUTHOR INFORMATION

Corresponding Author

*E-mail emma.harkonen@helsinki.fi.

Notes

The authors declare no competing financial interest.

ACKNOWLEDGMENTS

The research leading to these results has received funding from the European Community's Seventh Framework Program (FP7/2007−2013) under grant agreement no. CP-FP 213996-1. Academy of Finland (Finnish Centre of Excellence in Atomic Layer Deposition) is also thanked for support, and Region Ile-de-France is acknowledged for partial support for the ToF-SIMS equipment.

REFERENCES

(1) Sproul, W. D. *Surf. Coat. Technol.* **1996**, *81*, 1−7.
(2) Kelly, P. J.; Arnell, R. D. *Vacuum* **2000**, *56*, 159−172.
(3) Hurkmans, T.; Lewis, D. B.; Brooks, J. S.; Münz, W.-D. *Surf. Coat. Technol.* **1996**, *86−87*, 192−199.
(4) Mayrhofer, P. H.; Tischler, G.; Mitterer, C. *Surf. Coat. Technol.* **2001**, *142−144*, 78−84.
(5) Lee, C. K. *Mater. Sci. Technol.* **2006**, *22*, 653−660.
(6) Vovoedin, A. A.; Rebholz, C.; Schneider, J. M.; Stevenson, P.; Matthews, A. *Surf. Coat. Technol.* **1995**, *73*, 185−197.
(7) Wang, D.-Y.; Chang, C.-L. *Thin Solid Films* **2001**, *392*, 11−15.
(8) Chang, Y.-Y.; Wang, D.-Y.; Chang, C.-H.; Wu, W. T. *Surf. Coat. Technol.* **2004**, *184*, 349−355.
(9) Panjan, P.; Kek Merl, D.; Zupanic, F.; Cekada, M.; Panjan, M. *Surf. Coat. Technol.* **2008**, *202*, 2302−2305.
(10) Jehn, H. A. *Surf. Coat. Technol.* **2000**, *125*, 212−217.
(11) Lewis, D. B.; Creasey, S. J.; Wüstefeld, C.; Ehiasarian, A. P.; Hovsepian, P. E. *Thin Solid Films* **2006**, *503*, 143−148.
(12) Novotny, V.; Staud, N. *J. Electrochem. Sci. Tech.* **1988**, *135*, 2931−2938.
(13) Zeng, A.; Liu, E.; Annergren, I. F.; Tan, S. N.; Zhang, S.; Hing, P.; Gao, J. *Diamond Relat. Mater.* **2002**, *11*, 160−168.
(14) Reinhard, C.; Ehiasarian, A. P.; Hovsepian, P. E. *Thin Solid Films* **2007**, *515*, 3685−3692.
(15) Chipatecua, Y. I.; Olaya, J. J.; Arias, D. F. *Vacuum* **2012**, *86*, 1393−1401.
(16) Ritala, M.; M. Leskelä, M. Atomic layer deposition. In *Handbook of Thin Film Materials*; Nalwa, H. S., Ed.; Academic Press: San Diego, CA, 2002; p 103−158.
(17) Ritala, M.; Niinistö, J. Atomic layer deposition. In *Chemical Vapour Deposition: Precursors, Processes and Applications*; Jones, A. C., Hitchman, M. L., Eds.; The Royal Society of Chemistry: Cambridge, U.K., 2009; pp 158−206.
(18) Ritala, M.; Leskelä, M.; Dekker, J.-P.; Mutsaers, C.; Soininen, P. J.; Skarp, J. *Chem. Vap. Deposition* **1999**, *5*, 7−9.

(19) Matero, R.; Ritala, M.; Leskelä, M.; Salo, T.; Aromaa, J.; Forsén, O. *J. Phys. IV (France)* **1999**, *9*, Pr8−493−Pr8−499.
(20) Shan, C. X.; Hou, X.; Choy, K.-L. *Surf. Coat. Technol.* **2008**, *202*, 2399−2402.
(21) Marin, E.; Lanzutti, A.; Andreatta, F.; Lekka, M.; Guzman, L.; Fedrizzi, L. *Corros. Rev.* **2011**, *29*, 191−208.
(22) Díaz, B.; Światowska, J.; Maurice, V.; Seyeux, A.; Normand, B.; Härkönen, E.; Ritala, M.; Marcus, P. *Electrochim. Acta* **2011**, *56*, 10516−10523.
(23) Marin, E.; Lanzutti, A.; Guzman, L.; Fedrizzi, L. *J. Coat. Technol. Res.* **2011**, *8*, 655−659.
(24) Marin, E.; Guzman, L.; Lanzutti, A.; Ensinger, W.; Fedrizzi, L. *Thin Solid Films* **2012**, *522*, 283−288.
(25) Potts, S. E.; Schmalz, L.; Fenker, M.; Díaz, B.; Światowska, J.; Maurice, V.; Seyeux, A.; Marcus, P.; Radnóczi, G.; Tóth, L.; Kessels, W. M. M. *J. Electrochem. Soc.* **2011**, *158*, C132−C138.
(26) Díaz, B.; Härkönen, E.; Światowska, J.; Maurice, V.; Seyeux, A.; Marcus, P.; Ritala, M. *Corros. Sci.* **2011**, *53*, 2168−2175.
(27) Díaz, B.; Härkönen, E.; Światowska, J.; Maurice, V.; Seyeux, A.; Ritala, M.; Marcus, P. *Electrochim. Acta* **2011**, *56*, 9609−9618.
(28) Härkönen, E.; Díaz, B.; Światowska, J.; Maurice, V.; Seyeux, A.; Vehkamäki, M.; Sajavaara, T.; Fenker, M.; Marcus, P.; Ritala, M. *J. Electrochem. Soc.* **2011**, *158*, C369−C378.
(29) Díaz, B.; Światowska, J.; Maurice, V.; Seyeux, A.; Härkönen, E.; Ritala, M.; Tervakangas, S.; Kolehmainen, J.; Marcus, P. *Electrochim. Acta* **2013**, *90*, 232−245.
(30) Härkönen, E.; Díaz, B.; Światowska, J.; Maurice, V.; Seyeux, A.; Fenker, M.; Tóth, L.; Radnóczi, G.; Marcus, P.; Ritala, M. *Chem. Vap. Deposition* **2013**, *19*, 194−203.
(31) Härkönen, E.; Potts, S. E.; Kessels, W. M. M.; Díaz, B.; Seyeux, A.; Światowska, J.; Maurice, V.; Marcus, P.; Radnóczi, G.; Tóth, L.; Kariniemi, M.; Niinistö, J.; Ritala, M. *Thin Solid Films* **2013**, *534*, 384−393.
(32) Marin, E.; Lanzutti, A.; Guzman, L.; Fedrizzi, L. *J. Coat. Technol. Res.* **2012**, *9*, 347−355.
(33) Wang, P. C.; Shih, Y. T.; Lin, M. C.; Lin, H. C.; Chen, M. J.; Lin, K. M. *Thin Solid Films* **2010**, *518*, 7501−7504.
(34) Abdulagatov, A. I.; Yan, Y.; Cooper, J. R.; Zhang, Y.; Gibbs, Z. M.; Cavanagh, A. S.; Yang, R. G.; Lee, Y. C.; George, S. M. *ACS Appl. Mater. Interfaces* **2011**, *3*, 4593−4601.
(35) Chang, M. L.; Cheng, T. C.; Lin, M. C.; Lin, H. C.; Chen, M. *J. Appl. Surf. Sci.* **2012**, *258*, 10128−10134.
(36) Paussa, L.; Guzman, L.; Marin, E.; Isomäki, N.; Fedrizzi, L. *Surf. Coat. Technol.* **2011**, *206*, 976−980.
(37) Shan, C. X.; Hou, X.; Choy, K.-L.; Choquet, P. *Surf. Coat. Technol.* **2008**, *202*, 2147−2151.
(38) Marin, E.; Guzman, L.; Lanzutti, A.; Fedrizzi, L.; Saikkonen, M. *Electrochem. Commun.* **2009**, *11*, 2060−2063.
(39) Wang, P. C.; Cheng, T. C.; Lin, H. C.; Chen, M. J.; Lin, K. M.; Yeh, M. T. *Appl. Surf. Sci.* **2013**, *270*, 452−456.
(40) Härkönen, E.; Tervakangas, S.; Kolehmainen, J.; Díaz, B.; Światowska, J.; Maurice, V.; Seyeux, A.; Marcus, P.; Fenker, M.; Tóth, L.; Radnóczi, G.; Ritala To be published.
(41) Gordon, R. G.; Hausmann, D.; Kim, E.; Shepard, J. *Chem. Vap. Deposition* **2003**, *9*, 73−78.
(42) Fulem, M.; Ruzicka, K.; Ruzicka, V.; Hulicius, E.; Simecek, T.; Melichar, K.; Pangrac, J.; Rushworth, S. A.; Smith, L. M. *J. Cryst. Growth* **2003**, *248*, 99−107.
(43) Li, T.; Zhuang, W.-W.; Hsu, S. T. MOCVD precursors in mixed solvents. Eur. Pat. Appl.1184485, 2001
(44) L.J. Korb, L. J. In *Metals Handbook*, 9th ed.; ASM International: Materials Park, OH, 1987; Vol. *13*, p 17−36.
(45) Mendibide, C.; Steyer, P.; Millet, J.-P. *Surf. Coat. Technol.* **2005**, *200*, 109−112.
(46) Creus, J.; Mazille, H.; Idrissi, H. *Surf. Coat. Technol.* **2000**, *130*, 224−232.
(47) Massiani, Y.; Gravier, P.; Fedrizzi, L.; Marchetti, F. *Thin Solid Films* **1995**, *261*, 202−208.
(48) Wang, H. W.; Stack, M. M.; Lyon, S. B.; Hovsepian, P.; Münz, W.-D. *Surf. Coat. Technol.* **2000**, *126*, 279−287.
(49) Oh, J.; Myoung, J.; Bae, J. S.; Lim, S. *J. Electrochem. Soc.* **2011**, *158*, D217−D222.
(50) Färm, E.; Kemell, M.; Ritala, M.; Leskelä, M. *Thin Solid Films* **2008**, *517*, 972.
(51) Liu, J.; Mao, Y.; Lan, E.; Babtao, D. R.; Forse, G. J.; Lu, J.; Blom, H.-O.; Yeates, T. O.; Dunn, B.; Chang, J. P. *J. Am. Chem. Soc.* **2008**, *130*, 16908.
(52) George, S. M. *Chem. Rev.* **2010**, *110*, 111−131.
(53) Farmer, D. B.; Gordon, R. G. *Nano Lett.* **2006**, *6*, 699−703.
(54) Wang, X.; Tabakman, S. M.; Dai, H. *J. Am. Chem. Soc.* **2008**, *130*, 8152−8153.
(55) Robertson, J. *Mater. Sci. Eng.* **2002**, *R37*, 129−281.
(56) Robertson, J. *Semicond. Sci. Technol.* **2003**, *18*, S12−S19.